JOURNAL OF MATERIALS SCIENCE 22 (1987) 2767–2777

The intermediate transformation of Mn–Mo–Nb steel during continuous cooling

JYE-LONG LEE, MIN-HSIUNG HON
Department of Metallurgy and Materials Engineering, National Cheng Kung University, Tainan, Taiwan, ROC

GWO-HWA CHENG
R and D Department, China Steel Corporation, Kaohsiung, Taiwan, ROC

The continuous cooling transformation diagram for low-carbon low-alloy steel containing 0.05% C, 1.99% Mn, 0.31% Mo and 0.06% Nb was constructed by dilatometry and metallography. The intermediate transformation between martensite and polygonal ferrite involves two typical stages: the formation of ferrite matrix and the formation of microphases. Four intermediate transformation products obtained from various cooling rates and designated B_1, B_2, A_1 and A_2, were studied. The B_1 and B_2 structures are composed of pockets of parallel ferrite laths and interlath microphases, which are films of retained austenite in B_1 and are fragments of retained austenite or martensite or martensite-retained austenite (M–A) constituents in B_2. The B_1 structure is further characterized by the appearance of martensite particles inside the ferrite laths. The A_1 structure is comprised of the randomly arranged ferrite groups. Each group contains several short ferrite laths in the same crystallographic orientation and granular M–A constituents or martensite located at the rim of ferrite laths or groups. The A_2 structure is morphologically analogous to Widmanstätten ferrite. The formation mechanisms of these products are also discussed.

1. Introduction

The hot-rolled low-carbon Mn–Mo–Nb steel is well known for its superior combination of strength and toughness for potential use in arctic pipeline manufacturing [1–8]. The microstructure of these steels is characterized by the irregular and non-equiaxed ferrite grains with high dislocation density and trace amounts of cementite and islands of martensite. This type of microstructure is generally referred to as acicular ferrite [1–5, 7, 9].

The structural aspect of acicular ferrite has been controversial for a long time. Coldren and Mihelich [8] suggested that acicular ferrite was different from bainite for lack of prior austenite grain boundary. Collins *et al.* [9] deduced that the mechanism of acicular ferrite formation was similar to that of Widmanstätten ferrite based on the observations that the shape of acicular ferrite was irregular and there were many grain-boundary segments. In addition, several investigators [10, 11] concluded that acicular and bainitic ferrites were almost the same because their mechanical properties were so alike. That acicular ferrite might be produced through a bainitic or massive mechanism was proposed by Leslie [12]. However, these investigations shared the view that acicular ferrite is an intermediate transformation product between martensite and polygonal ferrite.

Referring to the intermediate transformation products, Widmanstätten ferrite, upper and lower bainites are well known in addition to granular bainite [13, 14]. However a comparison of the above intermediate transformation products with acicular ferrite was not thoroughly made. Most investigations of acicular ferrite were limited to hot-rolled steel, and it appears that no attention was drawn to the transformation products of unrolled steel with the similar composition. Furthermore, the investigations of continuous cooling transformation products of low alloy steels were conducted mostly for practical consideration; the range of cooling rate was very limited so that the whole range of intermediate transformation from polygonal ferrite to martensite was not fully investigated. Valuable observations and information may be missed and hence it is difficult to understand the formation aspect of acicular ferrite.

The purpose of the present investigation was to study the phase transformation of the most widely used acicular ferrite steel containing manganese, molybdenum and niobium at various cooling rates under unrolled state. Attempts were made to construct a continuous cooling transformation (CCT) diagram and to observe the microstructure of every possible intermediate transformation products for further understanding of the formation of acicular ferrite.

2. Experimental procedures

2.1. Materials

The steel used in this study was made from high purity electrolytic iron and ferroalloys. Melting was carried out in a vacuum induction furnace and the melt was

0022–2461/87 $03.00 + .12

TABLE I The chemical composition (wt %) of the Mn–Mo–Nb steel used

C	Si	Mn	P	S	Mo	Nb
0.051	0.210	1.990	0.016	0.023	0.310	0.059

cast into a 175 kg ingot. After having been reheated at 1200° C for 2 h, the ingot was fabricated to the 20 mm thick plate by controlled rolling. The chemical composition of the steel is given in Table I.

2.2. Dilatometric tests

Hollow cylindrical specimens of length 12 mm, outside diameter 5 mm and wall thickness 1 mm were cut from the plate transversely. The 0.13 mm diameter Pt–Pt 10% Rh thermocouple wires were welded to the specimens to ensure an accurate temperature measurement. The specimens were austenitized for 10 min at 1200° C in a vacuum of about 10^{-4} torr in the Theta high-speed dilatometer and subsequently cooled at various cooling rates. The cooling rates were carefully controlled by using a temperature programmer with the aid of regulated helium current to remove the latent heat evolved during the phase transformation. The specimens cooled at a rate slower than 900° C min^{-1} followed a constant cooling rate down to 150° C with a temperature deviation of no more than 10° C from the linear cooling curve at the transformation region. In the cases of doubtful data, double checks were made to enhance the reliability of the test.

2.3. Metallography

After dilatometric test, all specimens were mechanically polished and etched with 2% Nital etchant. Microstructural features were examined firstly by optical microscopy (OM). In order to examine the microstructure in more detail, the specimens were subjected to deep etching by prolonged holding in 2% Nital etchant, and were further investigated by scanning electron microscopy (SEM).

Thin-foil specimens for transmission electron microscopy (TEM) were mechanically grounded to about 100 μm and chemically thinned to about 60 μm. The final thinning was obtained using a jet electropolisher and an alcohol–15% perchloric acid electrolyte. The thin foils were examined in a Jeol CV II TEM at 100 kV.

3. Results

3.1. Continuous cooling transformation (CCT) diagram

In order to construct the complete CCT diagram for Mn–Mo–Nb steel, the cooling rates were varied from 10 to 30 000° C min^{-1}. The dilatation curves obtained were classified into three types as shown in Fig. 1.

As the cooling rate was slower than 66° C min^{-1}, the dilatation curve exhibited a three-stage dilational change as shown as Curve a in Fig. 1. In order to determine the transformation products formed at various stages, a series of interrupted quenching tests were carried out. The specimens were cooled at a rate of 55° C min^{-1} and subsequently interruptedly quenched

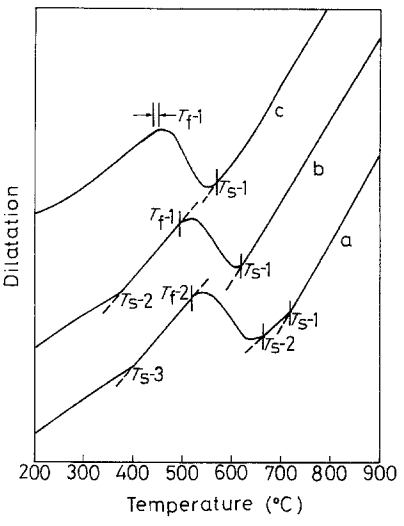

Figure 1 Types of dilatation curves. Cooling rates: Curve a, < 66° C min^{-1}; Curve b, 66 to 900° C min^{-1}; Curve c, > 900° C min^{-1}. T_s = transformation start temperature, T_f = transformation finish temperature.

at various temperatures during the transformation. Based on the microstructural observations, the polygonal ferrite was found to form firstly at about 720° C which is consistent with the temperature of the first-stage dilational change. The formation of ferrite matrix of the intermediate transformation product started at about 670° C and ceased at about 510° C. Both temperatures are compatible with the start and finish temperatures of the second-stage dilational change. The variation of volume fraction of polygonal ferrite and ferrite matrix of the intermediate transformation product with the quenching temperature is summarized in Fig. 2. The residual portion of the transformation product obtained from Curve a was found to be the microphases entrapped by the ferrite matrix of the intermediate transformation product. The microphases were found dominantly to be martensite or the combination of martensite and retained austenite through the examination of the TEM selected-area diffraction pattern. Hence, the final-stage dilational change corresponds to the post-transformation of austenite pools entrapped by ferrite matrix of the intermediate transformation product to martensite.

As the cooling rate fell between 66 and 900° C min^{-1}, the dilatation curve, shown as Curve b in Fig. 1, exhibited two dilational changes which were also

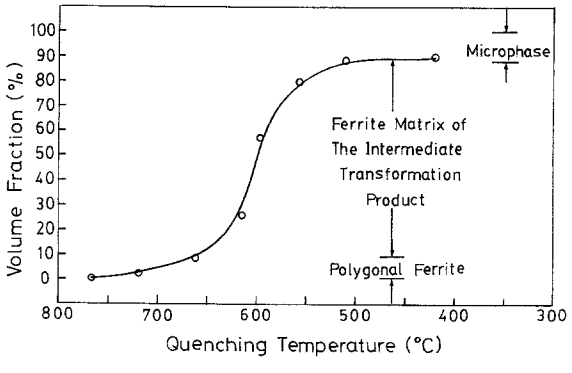

Figure 2 Variation of volume fraction of transformed ferrite with quenching temperature. Cooling rate before quenching = 55° C min^{-1}.

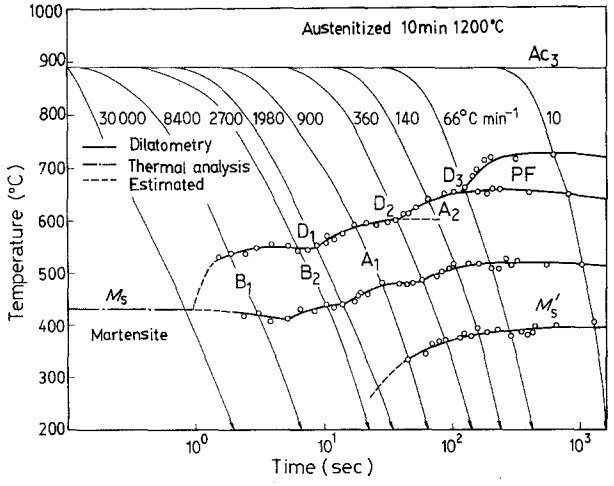

Figure 3 The CCT diagram for the Mn–Mo–Nb steel. PF = polygonal ferrite. (——) Dilatometry, (–●–) thermal analysis, (– – –) estimated.

checked by the interrupted quenching tests and corresponded to the formations of ferrite matrix and microphases of the intermediate transformation product, respectively. However, at a cooling rate greater than 900° C min^{-1}, the specimen did not follow a constant rate cooling path after the transformation had begun because the rate of latent heat evolved was so large that the regulated helium current was not able to remove the heat fast enough. In this case, the dilatational curve obtained (Curve c in Fig. 1) is of non-linear type and the transformation temperature of microphases was difficult to determine. Therefore, only the major transformation can be detected in Curve c.

The transformation diagram constructed from a large number of dilatation curves is shown by solid lines in Fig. 3. As can be seen, the transformation start temperature increases with decreasing cooling rate. At a cooling rate slower than 66° C min^{-1} (i.e. point D_3), the three transformation start lines corresponding to the three-stage dilational changes in the dilatation curve appear on the diagram (Fig. 3). These lines correspond to the formation of polygonal ferrite, ferrite matrix and microphases of the intermediate transformation products, respectively. When the cooling rate is increased to 30 000° C min^{-1}, the resultant structure as shown in Fig. 4a is martensite. The martensite transformation start temperature (M_s), determined from thermal analysis by a Gleeble 1500 machine, was found to be near 430° C.

Incidentally, between 30 000 and 66° C min^{-1}, there appear two discontinuous points at cooling rates of around 1980° C min^{-1} (i.e. Point D_1) and 360° C min^{-1} (i.e. point D_2), respectively, on the curve.

3.2. Metallographic examination of transformation products

3.2.1. Optical microscopy

The transformation product obtained at a cooling rate of 30 000° C min^{-1} is a platelet structure, as shown in Fig. 4a. The structure is very similar to the typical low-carbon martensite reported by Marder and Krauss [15]. This structure is believed to be martensite.

The typical product obtained at a cooling rate of 8400° C min^{-1} consists of a number of packets in a grain. Each packet is composed of numerous parallel sheaves as shown in Fig. 4b. The width of a sheaf is about 1.0 μm as shown by a pair of opposite arrows A in Fig. 4b. This product is quite different from martensite and is designated B_1.

At a cooling rate of 2700° C min^{-1}, the structure shown in Fig. 4c is obtained. The fine and extremely long ferrite laths are separated by slightly etched and well-aligned microphases. As also can be seen, the laths mostly developed from the grain boundary. There are only few packets of laths in a grain, unlike in the B_1 structure where a grain has many packets. For the

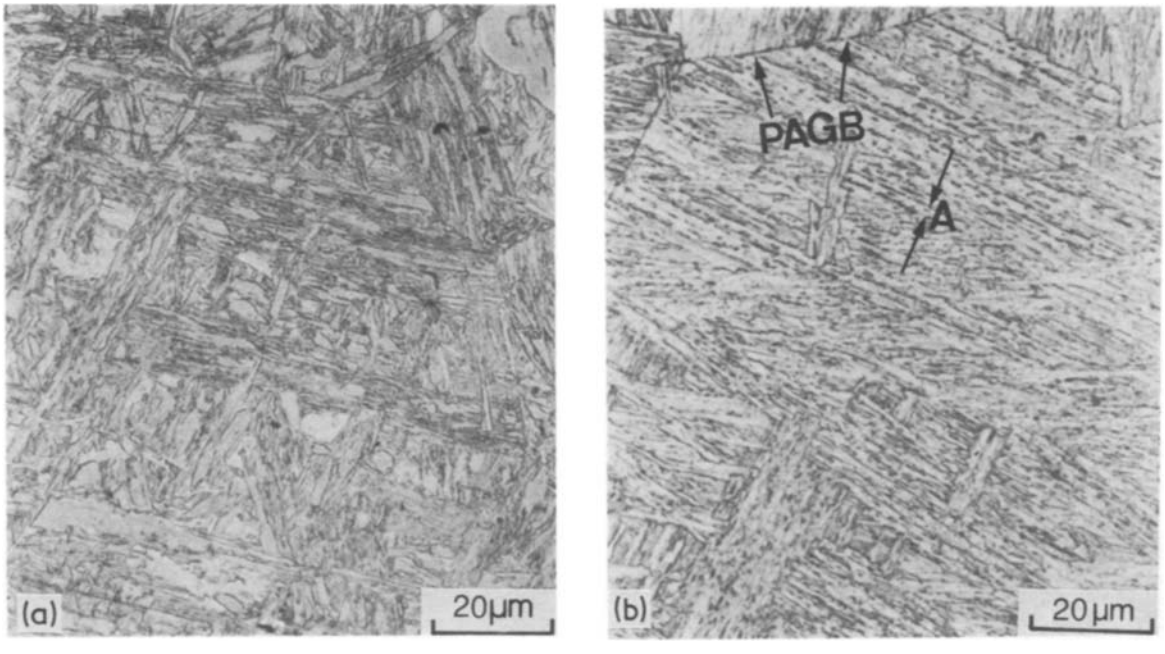

Figure 4 Optical micrographs obtained at various cooling rates: (a) 30 000, (b) 8400, (c) 2700, (d) 900, (e) 140, and (f) 55° C min^{-1}; PAGB = prior austenite grain boundary, A = an apparent sheaf, WF = Widmanstätten ferrite-like plates, PF = polygonal ferrite.

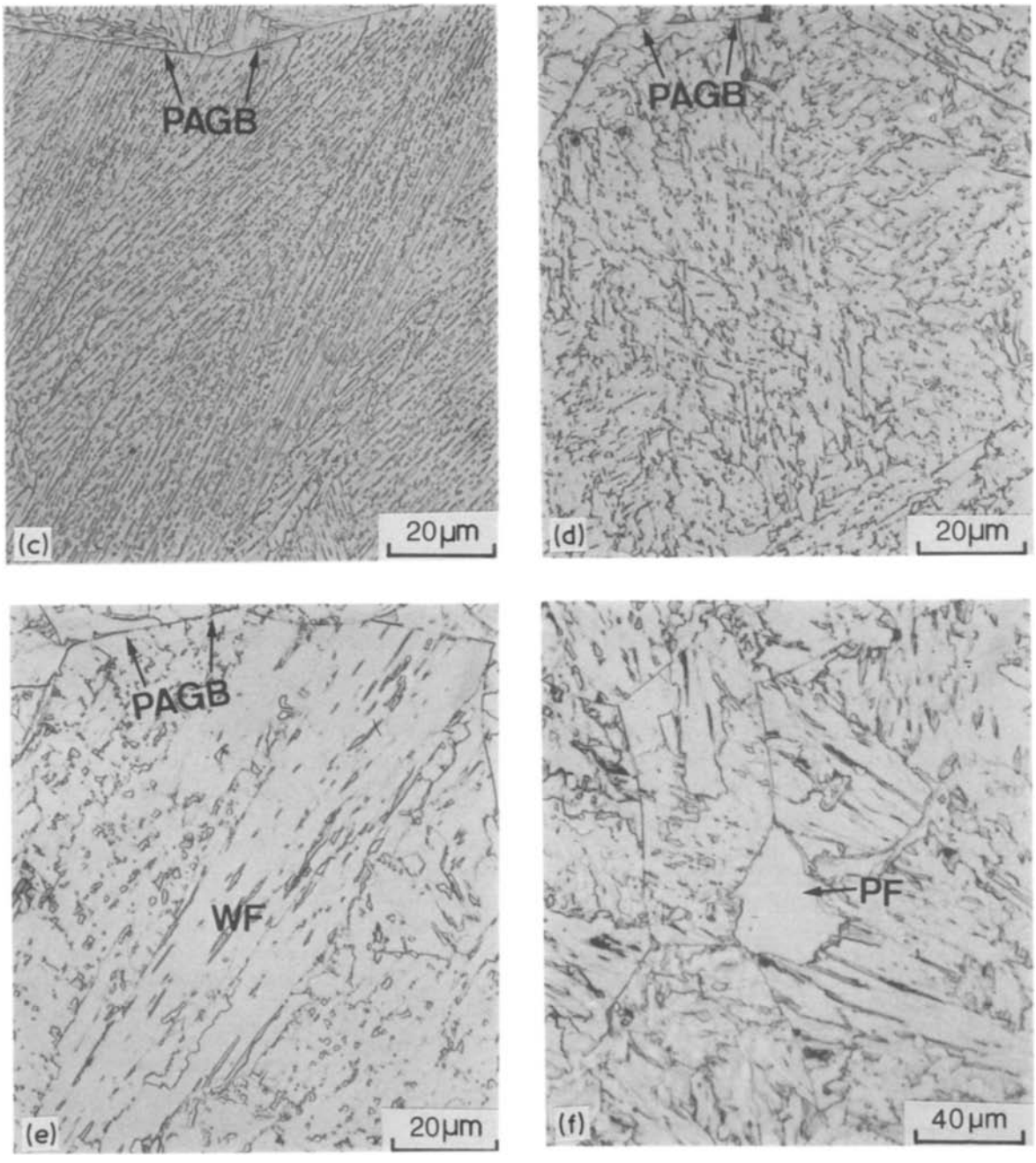

Figure 4 Continued.

convenience of further discussion, this structure is designated B_2.

The essential structure formed between points D_1 and D_2 is comprised of many irregularly shaped ferrite aggregates in which many granular microphases are dispersed as shown in Fig. 4d. The boundaries between the ferrite aggregates are ragged, indistinct and veined in appearance. This structure is designated A_1.

At a cooling rate of $140^\circ C\,min^{-1}$, i.e. between points D_2 and D_3, a structure consisting of ferrite plates and microphases was obtained in addition to the A_1 structure (Fig. 4e). The plates have a long wedge appearance with relatively large width and aspect ratio and they can probably be considered as Widmanstätten ferrite [16]. This structure is designated A_2. Metallographical observations also show that there is only a small amount of A_2 structure in the products formed to the left-hand side of point D_2, while the cooling rate is slower than at point D_2, and the volume fraction of A_2 structure increases with decreasing cooling rate.

When the cooling rate is less than $66^\circ C\,min^{-1}$, i.e. to the right-hand side of point D_3, the polygonal ferrite appears in the transformation product as shown in Fig. 4f. The polygonal ferrite is observed to grow across the prior austenite grain boundary. In addition, the second-stage transformation product was found to be Widmanstätten ferrite-like structure (A_2 structure) as shown in Fig. 4f.

3.2.2. SEM and TEM microscopy

The sheaf-like structure of B_1 exhibits a ragged surface with microphase films located at the ridge and some obscure boundary tracers at the valley as shown in the scanning electron micrograph, Fig. 5. Each band shown as A in Fig. 5 is 0.7 to 1.2 μm wide and is roughly equal to the width of a sheaf in the optical microscopy. At

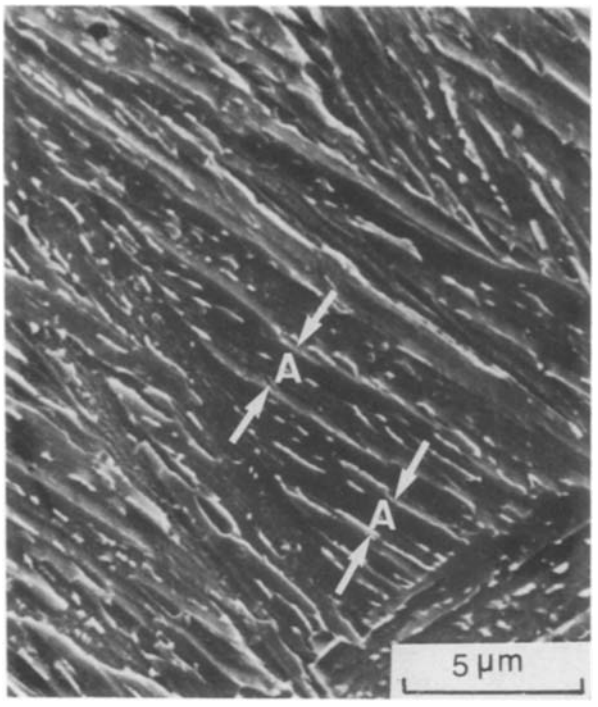

Figure 5 Scanning electron micrograph of the B_1 structure after deep etching.

higher magnification in the TEM micrograph, it is revealed that two to four fine ferrite laths appear in a width of the order of a sheaf as shown in Fig. 6a. The boundaries of these laths are frequently covered with layers of microphases (Fig. 6b) which were identified as retained austenite by the selected-area diffraction pattern technique. After the specimen was carefully tilted, some particles were found inside the ferrite lath and oriented at a large angle to the long axis of ferrite lath, as shown in Figs 6c and d. These particles were identified as martensite through the examination of the selected-area diffraction pattern. A trace amount of carbides was also found in the ferrite laths.

SEM of B_2 structure (Fig. 7) shows the alternate occurrence of ferrite laths and interlath microphases which are in linear fragmentary appearance and well aligned. It should be noted that the lath boundaries were only very slightly etched and the overall surface is flat. It can be demonstrated from the selected-area diffraction pattern that the adjacent laths are almost in the same crystallographic orientation. The fragmentary microphases were identified as retained austenite (Fig. 8a), or dislocated martensite (Fig. 8b) or twinned martensite (Figs 8c and d) from the selected-area diffraction patterns. However, some fragments were found to be comprised of martensite and retained austenite, i.e. so-called M–A constituents [17].

The SEM examination of the deep-etched A_1 structure which was veined in appearance in the optical micrograph clearly reveals that most of the microstructural units are short ferrite laths with aspect ratio about 3 to 6 as shown in Fig. 9. It is important to note that there is a distinct trend in which three to five laths or more get together to form a group. The group boundaries are irregular and have many protrusions or boundary segments. Moreover, the groups are in random arrangement. Most of the microphases are granular in form and located at the rim of laths or

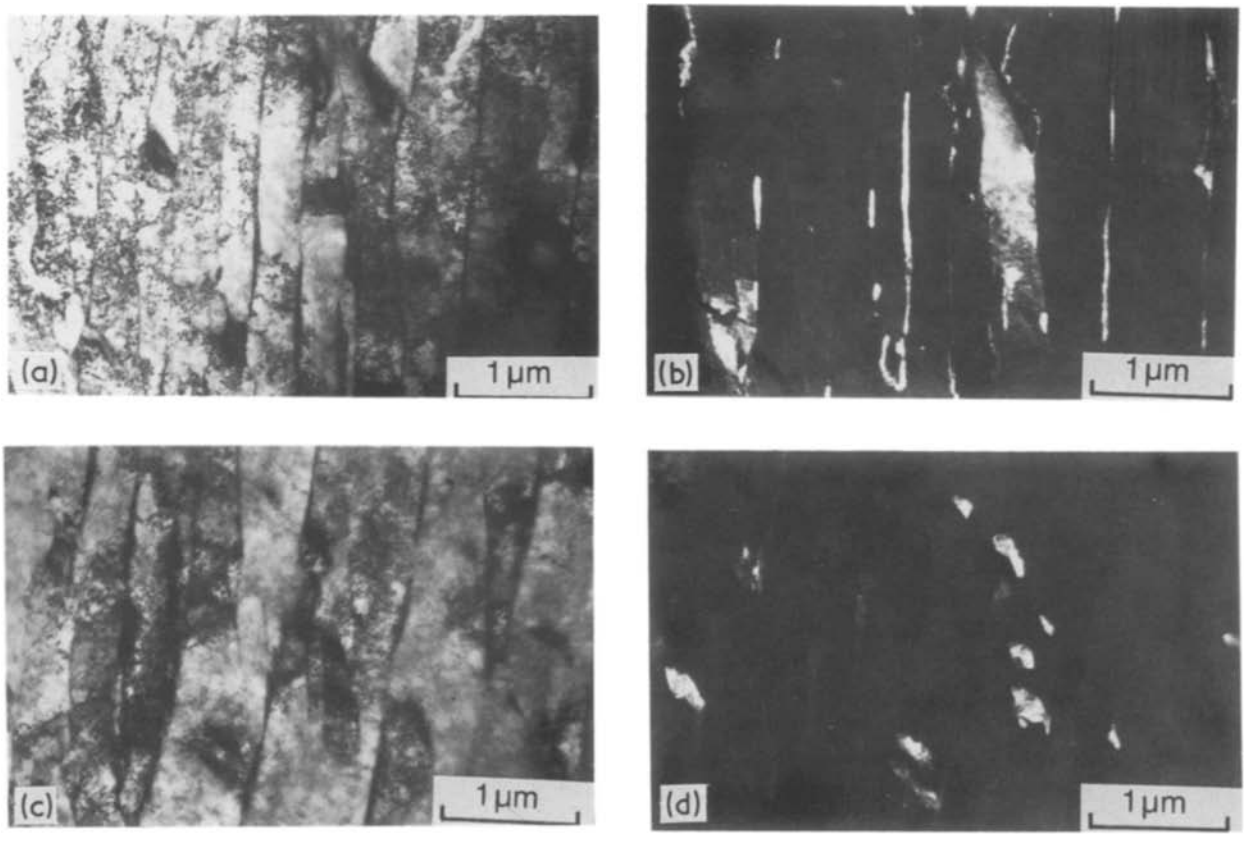

Figure 6 Transmission electron micrographs of the B_1 structure: (a) the bright-field image showing the fine ferrite laths, (b) the corresponding dark-field image of (a) showing interlath retained austenite films, (c) the bright-field image showing sub-unit ferrite laths and intralath martensite particles: (d) the corresponding dark-field image of (c) showing intralath martensite particles.

Figure 7 Scanning electron micrograph of the B_2 structure after deep etching.

groups. It was found that most of the microphases are martensite or M–A constituents, whereas the microphase existing as retained austenite alone was scarcely found. The transmission electron micrograph, Fig. 10a, shows that all the short ferrite laths possess a very high density of dislocations and their boundaries appear to be slightly curved. By the selected-area diffraction pattern technique, the adjacent laths A, B and C were found to have the same crystallographic orientation, while laths D and E have a different orientation. These features can also be demonstrated by dark-field image technique [18] as shown in Figs 10b and c. Apparently, the laths belonging to a group in the A_1 structure have almost the same crystallographic orientation and hence the groups can readily be identified in the scanning electron micrograph.

4. Discussion

4.1. Characteristics of intermediate transformation and its products

Based on the dilatometric experiments, interrupted quenching tests and metallographical observations, it was found that the intermediate transformation of Mn–Mo–Nb steel between martensite and polygonal ferrite proceeds via the following stages: the ferrite matrix forms first; subsequently, the resultant carbon-enriched austenite pools entrapped by the ferrite matrix transform to martensite or are retained by themselves. That the pools are carbon-enriched is clearly shown by the depression of their martensite transformation start temperature (line M_s' in Fig. 3) and by the twinned martensite observed in the B_2 structure (Figs 8c and d). The carbon enrichment of the austenite pool is believed to be a result of the carbon partition during the formation of the ferrite matrix. This transformation behaviour is very similar to the continuous cooling bainite transformation of low-carbon alloy steel as reported by Bojarski and Bold [19].

It was found that the prior austenite grain boundaries are retained in all the intermediate transformation products, as shown in Figs 4b, c, d and e. This implies that the semi-coherent or coherent interface [20] is operative during the nucleation of these products. However, the polygonal ferrite follows the non-coherent nucleation mode because it grows across the grain boundary (Fig. 4f). In addition, the ferrite matrix of all the intermediate transformation

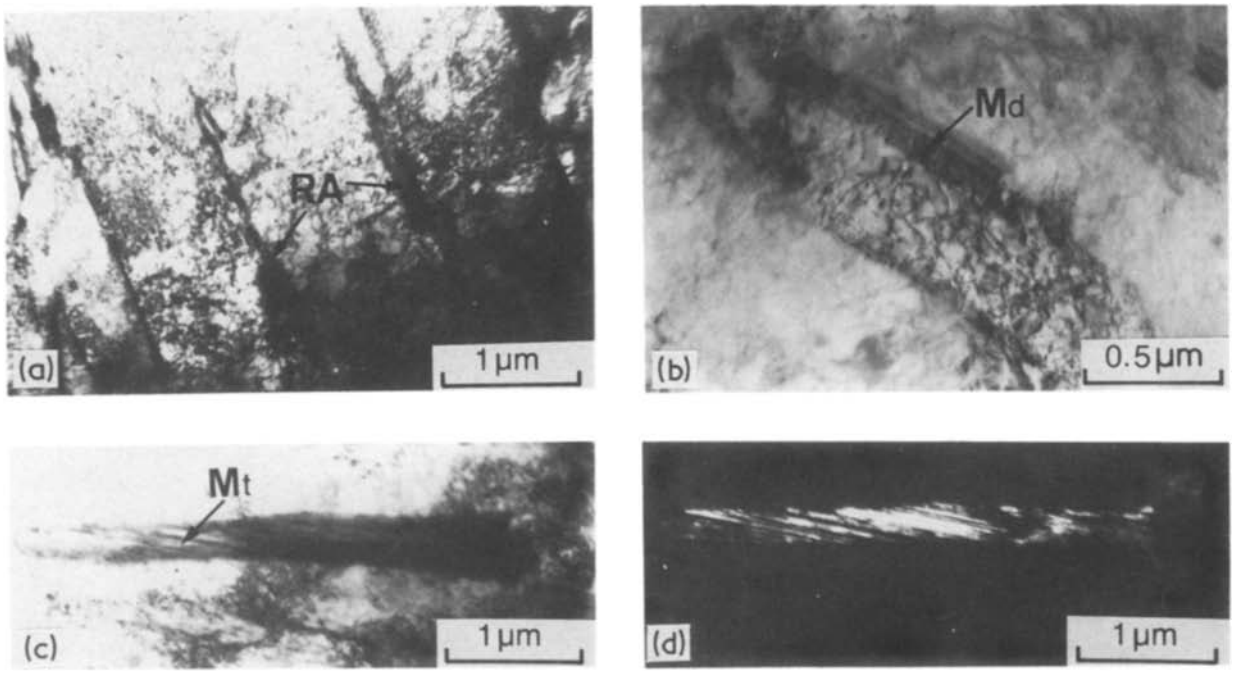

Figure 8 Transmission electron micrographs of the interlath microphases in the B_2 structure: (a) the bright-field image of retained austenite (RA), (b) the bright-field image of dislocated martensite (Md), (c) and (d) the bright-field image and the corresponding dark-field image of the twinned martensite (Mt).

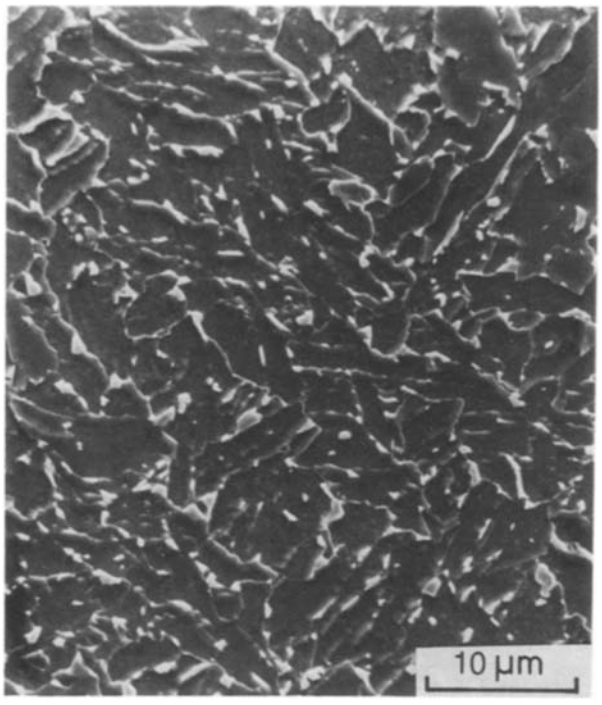

Figure 9 Scanning electron micrograph of the A_1 structure after deep etching.

products contains quite a high density of dislocations (Figs 6, 8, 10). It is believed that dislocations are induced by the transformation strain associated with the low-temperature transformation.

However, the B_1 and B_2 structures are different in surface flatness as shown by scanning electron micrographs (Figs 5 and 7) and in the microstructures of interlath microphases (Figs 6 and 8) although they are very similar in the sense of ferrite lath morphology. Moreover, the intralath martensite particles found in the B_1 structure were seldom detected in the B_2 structure. The A_1 structure containing randomly arranged groups (Fig. 9) is remarkably different from the B_2 structure. The latter is characterized by large-area directional growth (Figs 4c and 7). In addition, the microphases in the A_1 structure are granular and dispersive (Fig. 9), while those in B_2 are straight, fragmentary and well aligned (Fig. 7). The A_2 structure was morphologically analogous to Widmanstätten ferrite [16]. The structure is readily distinguished from the A_1 structure as it has a relatively large width and aspect ratio (Fig. 4e).

The possible reasons to cause the differences among the ferrite matrices and microphases of the intermediate transformation products will be discussed in the following sections.

4.2. The formation of ferrite matrix

It has been proposed by Oblak and Hehemann [21] that the bainite transformation is initiated by the formation of a ferrite unit and continues by repeated face-on-face nucleations of new ferrite units. The transmission electron micrograph, Fig. 6a, shows that each sheaf (shown as A in Fig. 4b) of the B_1 structure is actually comprised of several parallel ferrite laths. In addition, Fig. 6c shows that each apparent lath in Fig. 6a is a linear assemblage of many ferrite units. This structural feature suggests that the B_1 structure is also formed by repeated face-on-face nucleation. Figs 4c and 7 show that each packet of the B_2 structure is also comprised of many parallel extremely long apparent ferrite laths. Through the TEM metallographical observations, each extremely long apparent ferrite lath was found to contain many aligned ferrite units. This indicates that the formation of B_2 structure is also accomplished by repeated face-on-face nucleation. Moreover, the B_2 structure is believed to initiate the nucleation dominantly at grain boundaries because each prior austenite grain contains only a few ferrite packets which developed mostly from the grain boundary (Fig. 4c). However, the B_1 structure contains many intersecting packets within a grain (Fig. 4b). It demonstrates that, at relatively lower transformation temperature, the B_1 structure initiates the nucleation both inside the grain and at the grain boundary. This result is consistent with the expectation of the nucleation theory [22] that the intragranular nucleation tends to become more remarkable when transformation occurs at lower temperature.

Furthermore, the surface flatness of ferrite matrix of the B_1 and B_2 structures is quite different as shown by scanning electron micrographs (Figs 5 and 7). Based on the theoretical analysis proposed by Bhadeshia [23], the formation of two adjacent laths is most energetically favourable if they grow in the same crystallographic orientation. In the B_2 structure, the laths in a given packet were found almost in the same crystallographic orientation and the laths are therefore separated by low-angle lath boundaries. This suggests that the transformation associated with lower driving force prefers a co-orientation growth of adjacent laths due to the energetical consideration. Through TEM examinations, the adjacent laths in the B_1 structure were not always found in the same crystallographic orientation and then the frequency of laths being separated by high-angle boundaries is increased. This is reasonable, because transformation variants other than co-orientation growth are expected to be activated by a relatively large driving force associated with the lower temperature transformation.

The change in microstructures from B_2 to A_1 was found to take place gradually as shown in Fig. 11. The microstructure in Fig. 11a, which was obtained at a cooling rate of 2300° C min^{-1}, i.e. slightly slower than the cooling rate of B_2, very much resembles the B_2 structure except that more perpendicular intersecting packets were observed. When the cooling curve passes through point D_1, the number of perpendicular packets in a grain of the transformation product is further increased and the aspect ratio of an apparent lath is reduced (Fig. 11b). The microstructure of perpendicular packets suggests that the nucleation mode might follow the edge-on-face nucleation mode. The edge-on-face nucleation mode has been reported to be comparable to the face-on-face nucleation mode as the transformation temperature is increased [24]. As the cooling rate is slower than at point D_1, Fig. 11c shows that the arrangement of ferrite laths is more irregular and the lath boundaries become curved.

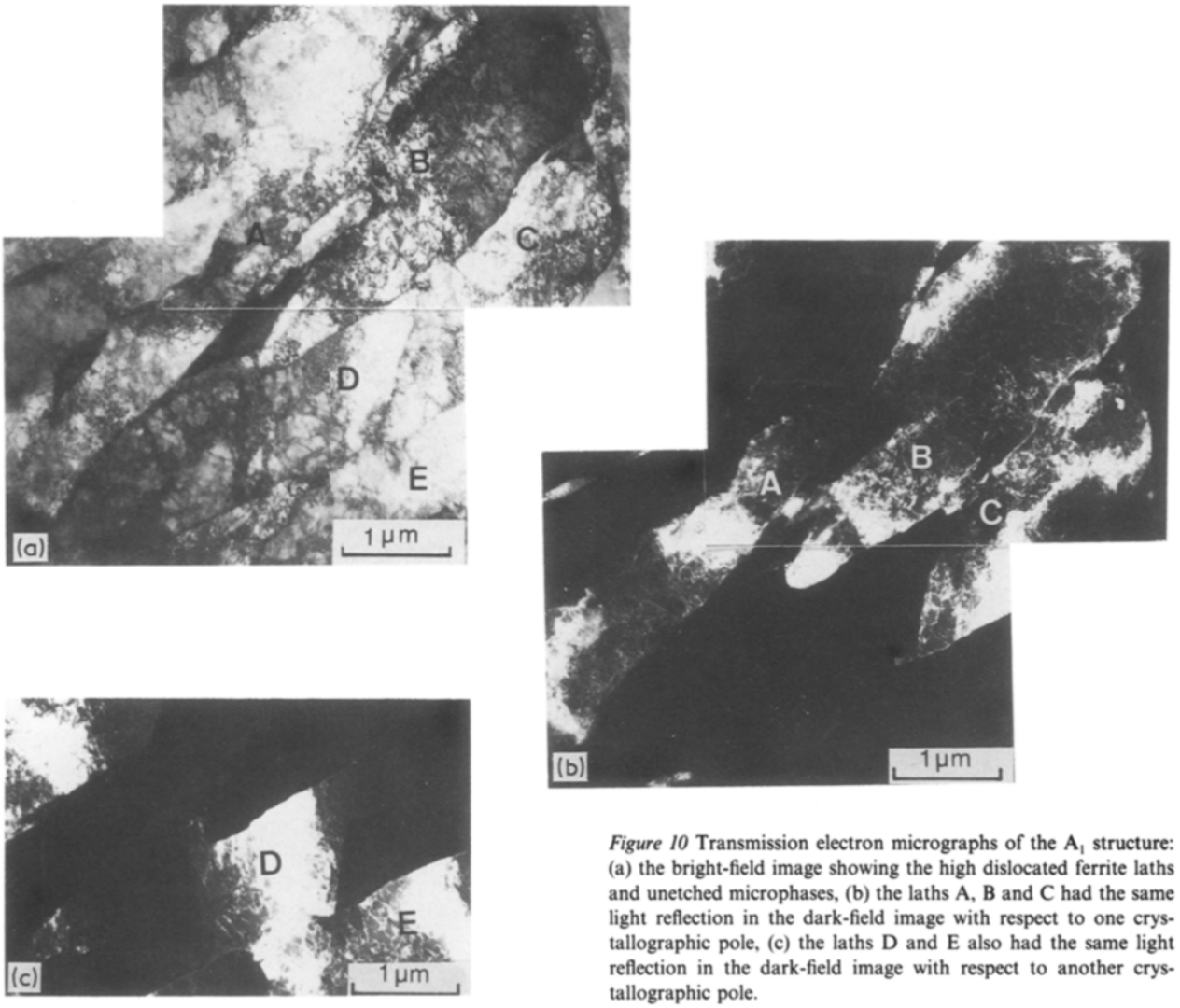

Figure 10 Transmission electron micrographs of the A_1 structure: (a) the bright-field image showing the high dislocated ferrite laths and unetched microphases, (b) the laths A, B and C had the same light reflection in the dark-field image with respect to one crystallographic pole, (c) the laths D and E also had the same light reflection in the dark-field image with respect to another crystallographic pole.

It might be attributed to the fact that the phase transformation occurring at higher temperature becomes more diffusional and less shear. Consequently, the A_1 structure formed at relatively higher temperature exhibits many randomly arranged groups in a grain (Fig. 9).

The A_2 structure was observed to grow from the grain boundary and looks like Widmanstätten ferrite. Through the TEM observations, no indication of the aggregate of ferrite subunits in a ferrite plate of the A_2 structure is seen. This suggests that the A_2 structure, like Widmanstätten ferrite, could be developed by the continued advance of a unique interface rather than by repeated nucleation [21].

4.3. The formation of microphases

In the present work, it is interesting to note that several kinds of interlath microphases are contained in the intermediate transformation products. They can be retained austenite in the B_1 structure, become retained austenite, martensite or M–A constituents in the B_2 structure and exist as martensite or M–A constituents in the A_1 structure at higher, intermediate and lower cooling rate, respectively. This trend seems to be consistent with the results of dilatometric tests which show that the martensite transformation start temperature (M_s') of carbon-enriched austenite pools decreases with increasing cooling rate (line M_s' in Fig. 3). If the M_s' temperature of the pools is so depressed to lower than room temperature, the pools would cease to transform.

It has been proposed by Hehemann *et al.* [25], that the carbon content of austenite adjacent to the growing ferrite can be determined from the extrapolated $(\alpha + \gamma)/\gamma$ boundary in the metastable equilibrium diagram. Subsequently, the interlath austenite resulting from a higher cooling rate would therefore be allowed more carbon enrichment at the lower transformation temperature. The austenite containing a higher carbon content is more resistant to the transformation to martensite.

On the other hand, it has been proposed that the stabilization of austenite can be attributed to the mechanical effect [26–28], i.e. the stability of austenite is determined by the accommodation strain energy required for martensitic transformation. In this regard, the stability of an austenite pool is sensitive to its size and shape, i.e. the small and thin pool tends to remain as austenite, because much more strain energy is required for the thin pool to transform to martensite [28]. The reasoning is compatible with the present observations in which the thin and small austenite

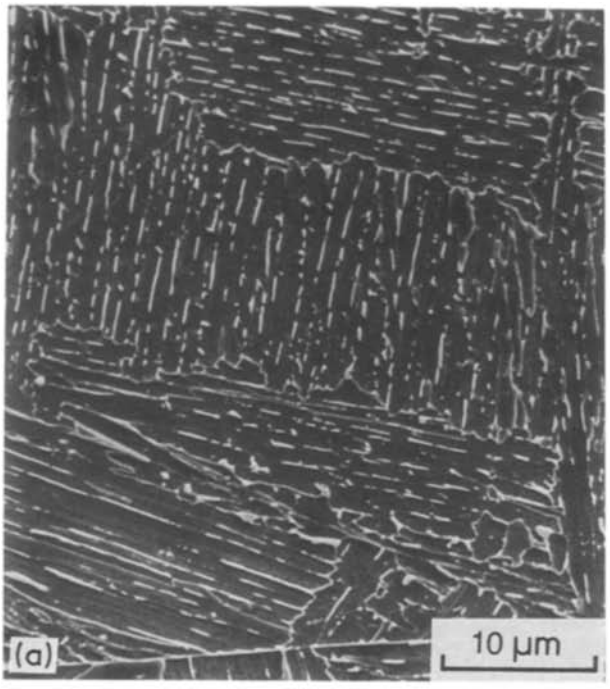

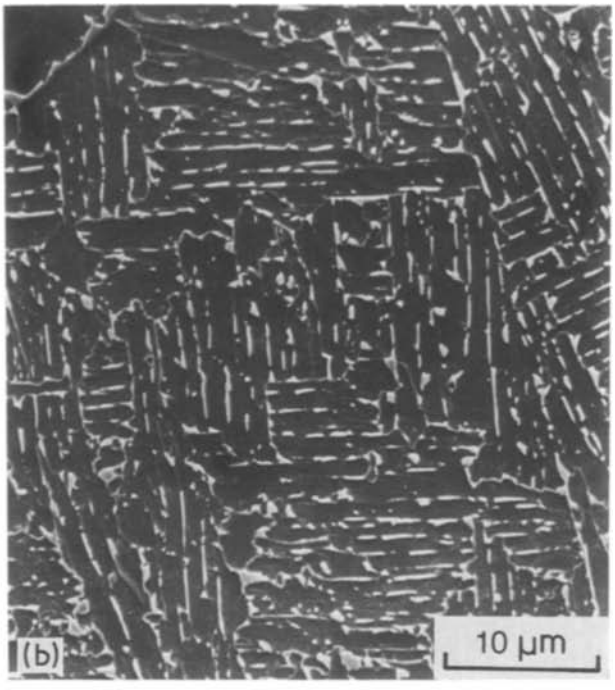

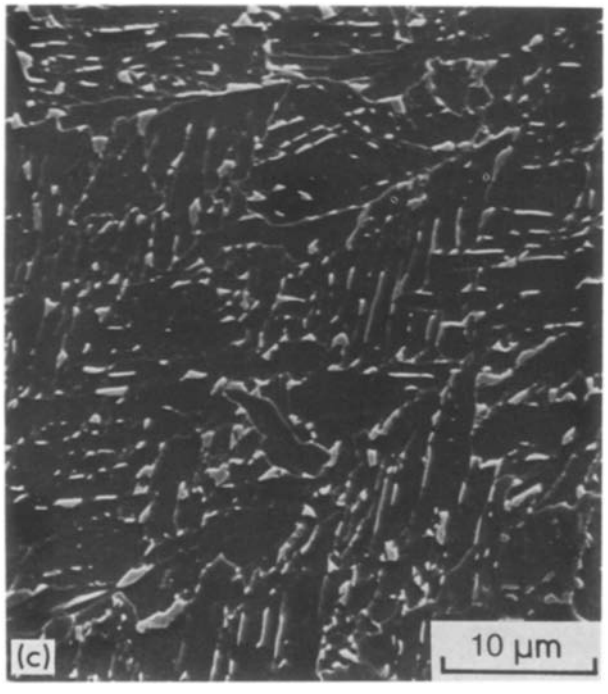

Figure 11 Scanning electron micrographs for the transformation products obtained at cooling rates of (a) 2300, (b) 1980 and (c) 1200° C min^{-1}.

pools, such as those in the B_1 and B_2 structures, tend to remain as retained austenite.

It should be noted that the intralath microphases found in the B_1 structure are martensite while the interlath microphases of the same transformation product are retained austenite. It seems that this can also be explained by mechanical stabilization. According to Fultz and Morris [28], the remaining austenite with a relatively large volume/surface ratio would require less strain energy for martensitic transformation. Therefore, the intralath-remaining austenite pools with a relatively larger volume/surface ratio than that of interlath austenite, transform more easily.

4.4. Occurrence of discontinuous points on CCT curve

There appear two discontinuous points, D_1 and D_2, between martensite and polygonal ferrite on the CCT curve (Fig. 3) which was constructed by repeated experiments. The metallographical observations show that only a small amount of A_2 structure is contained in the products formed to the left-hand side of point D_2. In the transformation products to the right-hand side of point D_2, the volume fraction of A_2 structure increases with decreasing cooling rate. In addition, as discussed in Section 4.2, the formation mechanisms of the ferrite matrix of both the A_1 and A_2 structures are quite different. Hence, it may be suggested that the occurrence of point D_2 is caused by the structural change from A_1 to A_2.

However, based on the discussion in previous sections, why point D_1 should be a discontinuous point is not known. Although there appear some differences in the formation of both ferrite matrix and the microphases between the B_2 and A_1 structures, the structural change from B_2 to A_1 only takes place gradually (Fig. 11). Therefore, further investigation is required on the occurrence of point D_1.

4.5. The B_1, B_2 structures and bainite

The B_1 and B_2 structures are very similar to the low-carbon upper bainite in the sense of the alternative appearance of parallel ferrite laths and interlath microphases (Figs 5 and 7). Their nucleation mode is also comparable as mentioned previously. However, the microphases in the B_1 and B_2 structure are retained austenite, martensite or M–A constituent instead of carbides in the conventional bainite. This should be attributed to the steel used in the present work being relatively high in manganese and molybdenum content. Both elements are capable of restraining austenite from decomposing into carbide [29]. The B_1 structure is further characterized by the existence of the intralath martensite particles (Fig. 6c), and this feature is of a similar fashion to the carbide

precipitations in lower bainite [30, 31]. However, it seems unsuitable to classify the B_1 structure as a lower bainite because the reaction temperature is so high that the lower bainite is unlikely to form. The lath structure of the B_1 structure (Fig. 6c) is also different from the ferrite plate in lower bainite. An upper bainite with the intralath carbide precipitations has been reported by Ohmori *et al.* [32]. The formation of intralath carbides in upper bainite was suggested simply as a result of the competition of carbon partition and the growth of bainitic ferrite. The appearance of intralath martensite in the B_1 structure might also result from a similar formation mechanism.

4.6. The A_1 structure and acicular ferrite

The A_1 structure is characterized by randomly arranged ferrite groups. The ferrite laths in a given group are in the same crystallographic orientation (Fig. 10). This feature suggests that the bainitic transformation mode, like that in the B_2 structure, still remains in local areas in the A_1 structure. Substantially, the veined structure in what appears to be an irregular ferrite grain as shown in Fig. 4d is, in fact, only the low-angle lath boundaries within the groups because they were not etched up distinctly.

It should be noted that there are many structural similarities between the A_1 structure and the acicular ferrite in the pipeline steel such as the veined appearance [1, 2, 6], non-equaxied ferrite grains with high dislocation density [3, 8], ferrite lath groups with many boundary protrusions [9] and the existence of M–A islands [8]. Moreover, among all the intermediate transformation products in this Mn–Mo–Nb steel, only the A_1 structure can be most probably related to the as-rolled acicular ferrite in the sense of microstructural similarities. Hence, it can be expected that the acicular ferrite and the A_1 structure are similar transformation products. In addition, the as-rolled acicular ferrite steels [2, 3, 8] possess very fine prior austenite grains resulting from the controlled rolling process and therefore, their transformation tends to start firstly by the formation of high-temperature transformation products, such as polygonal ferrite at grain boundaries. The prior austenite grain boundaries are then erased by these diffusional transformation products, as in the case of Fig. 4f, and the final products subsequently lack the prior austenite grain boundaries. This seems to be the reason why in the as-rolled acicular ferrite steels, the microstructure is generally very complicated.

5. Conclusions

1. The continuous cooling transformation diagram for low-carbon low-alloy steel containing 0.05% C, 1.99% Mn, 0.31% Mo and 0.06% Nb was constructed by dilatometric technique and metallographical observations. The intermediate transformation between martensite and polygonal ferrite involves two typical stages: the formation of ferrite matrix and the formation of microphases. Four typical intermediate transformation products obtained from various cooling rates and designated B_1, B_2, A_1 and A_2, respectively, were studied.

2. The B_1 structure is composed of many packets of parallel sheaves, each sheaf containing several fine ferrite laths. The boundaries of the laths are always covered with a layer of retained austenite. In addition, some martensite particles and a trace amount of carbides were also found inside the laths.

3. In the B_2 structure, there are only a few packets of parallel ferrite laths in a grain. The ferrite laths are separated by the aligned linear fragmentary interlath microphases which contain retained austenite, martensite or M–A constituents.

4. In the A_1 structure, there appear many randomly arranged ferrite groups in a prior austenite grain. Each group is comprised of several short ferrite laths in the same crystallographic orientation and granular microphases are located at the rim of laths or groups. The microphases are typically martensite or M–A constituents.

5. The A_2 structure is characterized by long wedge ferrite plates and is morphologically analogous to Widmanstätten ferrite plate.

6. The mechanisms of the formation of both the ferrite matrix and microphases in these intermediate transformation products were also discussed.

Acknowledgement

The authors are grateful to China Steel Corporation for financial support and permission to publish this paper.

References

1. Y. E. SMITH, A. P. COLDREN and R. L. CRYDERMAN, in "Toward Improved Ductility and Toughness" (Climax Molybdenum Co., Kyoto, Japan, 1971) p. 119.
2. R. L. CRYDERMAN, A. P. COLDREN, Y. E. SMITH and J. L. MIHELICH, in "Proceedings of 14th Mechanical Working and Steel Processing Conference, Vol. 10 (AIME, Chicago, Illinois, 1972) p. 114.
3. A. P. COLDREN, Y. E. SMITH and R. L. CRYDERMAN, in "Processing and Properties of Low Carbon Steel", edited by J. M. Gray, (AIME, New York, 1973) p. 163.
4. E. C. HAMRE and A. M. GILROY-SCOTT, "Microalloying 75", (Union Carbide Corp., New York, 1977) p. 375.
5. D. B. McCUTCHEON, T. W. TRUMPTER and J. D. EMBURY, *Rev. Met.* **73** (1976) 143.
6. D. S. DABKOWSKI and G. R. SPEICH, in "Mechanical Working and Steel Processing XV" (AIME, Pittsburgh, 1977) p. 284.
7. H. GONDOH, H. NAKASUGI, H. MATSUDA, H. TAMEHIRO and H. CHINO, Nippon Steel Technical Report No. 14 (1979) p. 55.
8. A. P. COLDREN and J. L. MIHELICH, in "Molybdenum — Containing Steels for Gas and Oil Industry Applications" (Climax Molybdenum Co. 1981) p. 14.
9. L. E. COLLINS, M. J. GODDEN and J. D. BOYD, *Can. Metall. Q.* **22** (1983) 169.
10. M. PONTREMOLI, P. BUFALINI, A. APRILE and C. JANNONE, *Met. Technol.* **11** (1984) 504.
11. R. L. CRYDERMAN, A. P. COLDREN, J. R. BEEL and J. D. GROZIER, *Trans. ASM* **63** (1969) 561.
12. W. C. LESLIE, in "The Physical Metallurgy of Steels" (McGraw-Hill, New York, 1981) p. 201.
13. L. J. HABRAKEN and M. ECONOMOPOULOS, in "Transformation and Hardenability in Steel" (Climax Molybdenum Co., 1967) p. 69.
14. F. H. SAMUEL, *Z. Metallkde* **75** (1984) 963.
15. A. R. MARDER and G. KRAUSS, *Trans. ASM* **60** (1967) 651.
16. R. D. TOWNSEND and J. S. KIRKALDY, *ibid.* **61** (1968) 605.

17. V. BISS and R. L. CRYDERMAN, *Met. Trans.* **2** (1971) 2267.
18. K. WAKASA and C. M. WAYMAN, *Metallogr.* **14** (1981) 49.
19. Z. BOJARSKI and T. BOLD, *Acta Metall.* **22** (1974) 1223.
20. C. S. SMITH, J. S. KIRKALDY and M. HILLERT, in "Decomposition of Austenite by Diffusional Processes", edited by V. F. Zackay and H. I. Aaronson (Interscience, New York, 1962) p. 197.
21. J. M. OBLAK and R. F. HEHEMANN, in "Transformation and Hardenability in Steels" (Climax Molybdenum Co., 1967) p. 15.
22. P. G. SHEWMON, in "Transformations in Metals" (McGraw-Hill, New York, 1969) p. 210.
23. H. K. D. H. BHADESHIA, *Acta Metall.* **29** (1981) 1117.
24. H. I. AARONSON and C. WELLS, *Trans. AIME* **206** (1956) 1216.
25. R. F. HEHEMANN, K. R. KINSMAN and H. I. AARONSON, *Met. Trans.* **3** (1972) 1077.
26. K. R. KINSMAN, G. DAS and R. F. HEHEMANN, *Acta Metall.* **25** (1977) 359.
27. M. SARIKAYA, G. THOMAS, J. W. STEEDS, S. J. BARNARD and G. D. W. SMITH, in "Solid to Solid Phase Transformations", edited by H. I. Aaronson, D. V. Laughlin, R. F. Sekerka and C. M. Wayman (AIME, New York, 1983) p. 1421.
28. B. FULTZ and J. W. MORRIS Jr, *Met. Trans.* **16A** (1985) 2251.
29. B. FULTZ, J. I. KIM, Y. H. KIM, H. J. KIM, G. O. FIOR and J. W. MORRIS Jr, *ibid.* **16A** (1985) 2237.
30. D. N. SHACKLETON and P. M. KELLY, in "Physical Properties of Martensite and Bainite", ISI Special Report 93, (Iron and Steel Institute, Randon, 1965) p. 135.
31. H. K. D. H. BHADESHIA, *Acta Metall.* **28** (1980) 1103.
32. J. OHMORI, H. OHTANI and T. KUNITAKE, *Trans. ISIJ* **11** (1971) 250.

Received 17 June 1986
and accepted 15 January 1987